



# Dielectric relaxation and thermally activated a.c. conduction in (PVDF)/(rGO) nano-composites: role of rGO over different fillers

Mervat Ismail Mohammed<sup>1</sup> · Suzan Salah Fouad<sup>1</sup> · Neeraj Mehta<sup>2</sup> 

Received: 5 July 2018 / Accepted: 23 August 2018 / Published online: 10 September 2018  
© Springer Science+Business Media, LLC, part of Springer Nature 2018

## Abstract

The present study describes the fabrication of nano-composites of (PVDF)/(rGO) using solution–cast method. We employed two characterizations for PVDF/rGO nano-composites, Scanning electron microscopy (SEM) and Fourier-transform infrared (FTIR) spectroscopy, the SEM indicates that the PVDF matrix consists of pores with the presence of globular structures that increases with the increasing rGO concentration, while the FTIR have been used to confirm the interplay between rGO and PVDF matrix. The dielectric measurements of PVDF/rGO nano-composites show a high dielectric constant and low dielectric loss factor. Moreover, frequency and temperature dependent behavior of a.c. conductivity has been carried out in the respective ranges of  $10^2$ – $10^6$  Hz and 303–393 K. Results of a.c. conductivity and the frequency exponent have been found to obey the theory of correlated barrier hopping. Further analysis shows that thermally assisted a.c. conduction shows the compensation effect. The role of rGO over other recent fillers is also summarized by a comparative tabulation of data available in the literature.

## 1 Introduction

In recent years, graphene has been acquired great attention because of their important electrical and thermal conductivity, in addition to its superior mechanical and promising performance properties [1–9]. However, the preparation of graphene has become one of the most intense fields of research due to the existence of van der Waals forces and the formation of the  $\pi$ -bond as well. Graphene oxide sheets are highly hydrophilic. Owing to the existence of functional groups containing oxygen (such as carbonyl, carboxyl, hydroxyl, epoxy groups [10]), Graphene oxide is dispersed in the different polar solvent [10]. The percolation theory suggests that Graphene can strengthen the dielectric parameters of the polymer [11, 12]. For the nano-composites, all the dielectric parameters of a polymer are enhanced when the concentration of the filler enters the percolation threshold [13]. PVDF, poly(vinylidene fluoride), has relatively good breakdown strength and high dielectric constant so,

it is considered a hopeful elasticity piezoelectric and ferroelectric materials. PVDF has a variety of crystalline phases, which characterize the ordered state for the dipoles through them; an extremely ordered state is displayed by  $\beta$ -phase for the entire trans (TTTT) arrangement where, all fluorine atoms are coordinated on one side, which achieved various technological applications [14]. The high dielectric constants were observed and the percolation thresholds were determined in some novel materials by using functionalized graphene for the preparation of nano-composites of poly(vinylidene fluoride) and poly(vinyl alcohol) [15].

Early studies verified the graphene as the conductive filler showing a lower percolation threshold and maximum dielectric constant of the nano-composite films [16–18]. It was found that the majority of these articles did not interested in studying the effect of concentration of conductive filler on other affecting parameters such as the percolation network near to the percolation threshold, the dielectric loss ( $\tan \delta$ ), and effect of the vacancy in the interface on the formation of a homogeneous composite. Therefore, it is interesting to study that how graphene nano-sheets control the dispersion throughout the matrix of polymer and their surface functionalization [19–23].

From above survey, it is clear that various literature is available on poly(vinylidene fluoride) (PVDF) and reduced graphene oxide (rGO) individually but only few studies are

✉ Neeraj Mehta  
dr\_neeraj\_mehta@yahoo.co.in

<sup>1</sup> Department of Physics, Faculty of Education, Ain Shams University, Cairo, Egypt

<sup>2</sup> Department of Physics, Institute of Science, Banaras Hindu University, Varanasi, India

available on the composites of both materials. Further, the available studies report the properties of PVDF/rGO nanocomposites in bulk form but here we have synthesized some novel samples in thin film form and succeeded in achieving high dielectric constant and low dielectric loss factor. These studies open a new gateway and new possibilities for improving the capacities of capacitors by using the nanocomposites, which are important for applications in nanoelectronics. In the present work, SEM and FTIR of PVDF/rGO nanocomposite films have been used to analyze the effect of doping on the surface morphology. Further, dielectric and a.c. conductivity have been measured and discussed.

## 2 Material and method

PVDF (granular) and rGO nano-particles of size less than 100 nm were taken from Karlsruhe (Germany) and Nano-Tech Egypt for Photo-Electronics respectively. The *N,N*-dimethylformamide (DMF) (supplied from Merck India Ltd) was utilized as the solvent by using the solution casting method. We used the films of five kinds of rGO–PVDF nanocomposite with diverse volume fractions of rGO, consisting of 0 vol%, 0.45 vol%, 0.9 vol%, 1.8 vol% and 2.7 vol% rGO loadings. The samples were prepared as follows, *N,N*-dimethylformamide (DMF) was used to dissolve PVDF using a magnetic stirrer at 60 °C for 12 h. The rGO nano-particles were dissolved according to the weight ratio in DMF then mixed drop by drop in a solution of PVDF to prepare PVDF–rGO nanocomposite films. Moreover, PVDF–rGO solution was stirred for 6 h to become homogeneous. An oven was used at room temperature for 24 h to produce the films by placing the solution with the petri dish inside the oven. We extracted the films from the petri dish and placed 7 days at room temperature to eliminate the remaining solvent. The volume fraction of rGO–PVDF ( $f_{vol}$ ) can be calculated by equation [15]:

$$f_{vol} = \frac{\varphi_{rGO}/\rho_{rGO}}{\varphi_{rGO}/\rho_{rGO} + (1 - \varphi_{rGO})/\rho_{PVDF}} \quad (1)$$

here  $\varphi_{rGO}$  illustrates the weight fraction of GO in PVDF matrix;  $\rho_{rGO}$ , and  $\rho_{PVDF}$  are the density of reduced graphene oxide (1.91 g/cm<sup>3</sup>), and PVDF (1.78 g/cm<sup>3</sup>). Nicolet 5700 spectrometer was used to measure infrared Fourier transform spectra (FT-IR). The morphologies of the samples were performed by a Quanta 250 FEG (field emission gun) microscope. We employed a programmable automatic LCR meter (Model FLUKE PM6306) for measuring the dielectric properties.

## 3 Results and discussion

### 3.1 Surface morphological characterization

The SEM analysis was performed to confirm the morphology of PVDF and rGO/PVDF nanocomposites. SEM images of PVDF at various volume contents of rGO are depicted in Fig. 1. It can be seen clearly in Fig. 1a that the pure PVDF has a rough surface with the pores having clear distinction in dimension and distribution of pores, while the SEM micrographs of composites with [0.9, 2.7 vol%] of rGO inset of Fig. 1b and c show small globules presence on the matrix corresponding to the rGO nano-particles, which are well dispersed and fully covered PVDF matrix. The sharing on the matrix surface is homogeneous and there are regions having product clusters that cover them entirely and others with a preponderance of PVDF. The PVDF matrix shows the formation of globular structures in their pores that can be seen when the rGO concentration is increased [24].

FTIR was used for the spectroscopy of the samples to further demonstrate the strong interplay between rGO and the PVDF matrix and its nanocomposites spectrum is shown in Fig. 2. From FTIR spectra, we observed the strong and sharp peaks at about 880, 840, 1270 and 1403 cm<sup>-1</sup>. These peaks can be revisited to the deformation vibrations and asymmetric stretching of C–H and the C–F of PVDF, respectively [25–27]. Also, we observed a band at 840 cm<sup>-1</sup> corresponding to a merged mode of CF<sub>2</sub> asymmetric stretching vibration and CH<sub>2</sub> rocking. At 2980 and 3020 cm<sup>-1</sup>, the absorption peak positions confirm the presence of the asymmetric CH<sub>2</sub> and symmetric vibration [28]. Owing to the FTIR spectrum the dipole–dipole interaction in PVDF/rGO is also conceivable. From the obtained analysis, it is evident that there is a physical interaction between the filler and polymer [29].

FTIR is usually used to determine the  $\beta$ -crystalline phases in a polymer and is expressed as [30]:

$$F(\beta) = \frac{X_{\beta}}{X_{\alpha} + X_{\beta}} = \frac{A_{\beta}}{(K_{\beta}/K_{\alpha})A_{\alpha} + A_{\beta}} \quad (2)$$

here  $K_{\alpha}$  and  $K_{\beta}$  represent the absorption coefficients corresponding to the individual wavenumber.  $K_{\alpha}$  is  $6.1 \times 10^4$  cm<sup>2</sup>/mol and  $K_{\beta}$  is  $7.7 \times 10^4$  cm<sup>2</sup>/mol.  $X_{\alpha}$  and  $X_{\beta}$  show the fractional mass of  $\alpha$  and  $\beta$  crystalline phases.  $A_{\alpha}$  and  $A_{\beta}$  are the absorption bands areas at 764 and 840 cm<sup>-1</sup>. The relative fraction for  $\beta$  phase utilizing the Eq. (2) are 60.37%, 61.9%, 62.5%, 63.85 and 65.68% for PVDF, PVDF/rGO nanocomposites, respectively. It has been found that  $\beta$ -phase has obvious increase with PVDF/rGO additives compared to pure PVDF. The refinement in the  $\beta$ -phase confirms that there is a good interaction of the additives with the fluorine in the polymer matrix. Another similar refinement behavior was reported earlier [31].

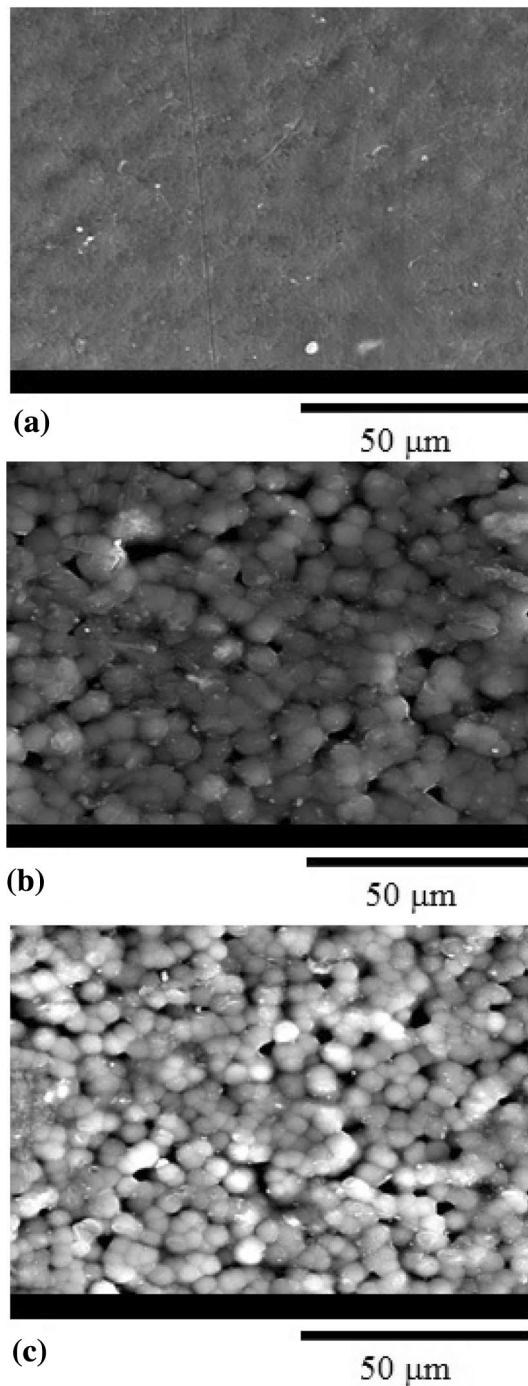


**Fig. 1** SEM micrographs of **a** PVDF, **b** rGO/PVDF ( $f=0.9$  vol%) and **c** rGO/PVDF ( $f=2.7$  vol%)

### 3.2 Dielectric properties

Thomas and his co-workers [32] enhanced the dielectric properties of poly(vinylidene fluoride) (PVDF) using  $\text{CaCu}_3\text{Ti}_4\text{O}_{12}$ . Zhuo et al. [33] studied the thermal conductivity and dielectric properties of Al/PVDF composites.

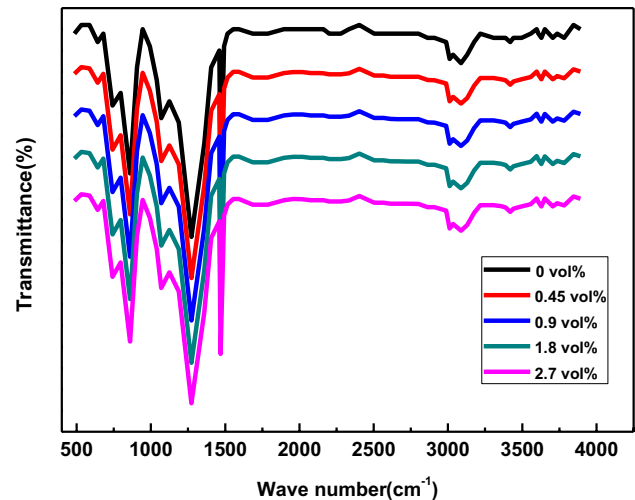


**Fig. 2** FT-IR spectra of PVDF polymer and nano-composite samples

Deng et al. [34] fabricated novel 2–3-type composites based on zinc powders and polyvinylidene fluoride. Yang and his group [35] enhanced dielectric and ferroelectric properties of flexible poly(vinylidene fluoride) by using  $\text{TiO}_2$ @MWCNTs nano-particles as filler. Dielectric properties of poly(vinylidene fluoride) nano-composites filled with surface coated  $\text{BaTiO}_3$  by  $\text{SnO}_2$  nanodots were reported by Zha et al. [36]. Li et al. [37], developed polyvinylidene fluoride (PVDF) composites having high dielectric constant and low loss tangent. For this purpose, they used graphene-encapsulated barium titanate hybrid fillers. Zhang et al. [38] and Li et al. [39] used nano iron oxide-deposited barium titanate hybrid particles and calcined  $\text{BaTiO}_3$  ceramic powders respectively for improving the dielectric properties of PVDF. The fillers nano-barium titanate/nickel hydroxide and plate-like  $(\text{Ba}_{0.6}\text{Sr}_{0.4})\text{TiO}_3$  were used by Yang et al. [40] and Wang et al. [41].

Under dielectric studies, the electrical properties were studied as a function of frequency and temperature. Dielectric analysis helps to define two fundamental parameters: the dielectric constant  $\epsilon'$  and the loss tangent, (dissipation factor). From the obtained results given in Fig. 3, it has been observed that  $\epsilon'$  decreases with increasing frequency as shown in Fig. 3a.

This frequency-dependent behavior can be also denoted to the interfacial polarization (Maxwell–Wagner–Sillars polarization). The increase of  $\epsilon'$  with the increase of rGO percentage can be understood in terms of the increase in volume fraction of conductive nano-filler in the PVDF matrix which further causes the slow formation of micro-capacitor networks [42, 43]. Also, the increase might be due to a large amount of aggregation between materials in an electric field that causes the dipoles to collide with each other and produces heat [44–46]. The dependence of the change of

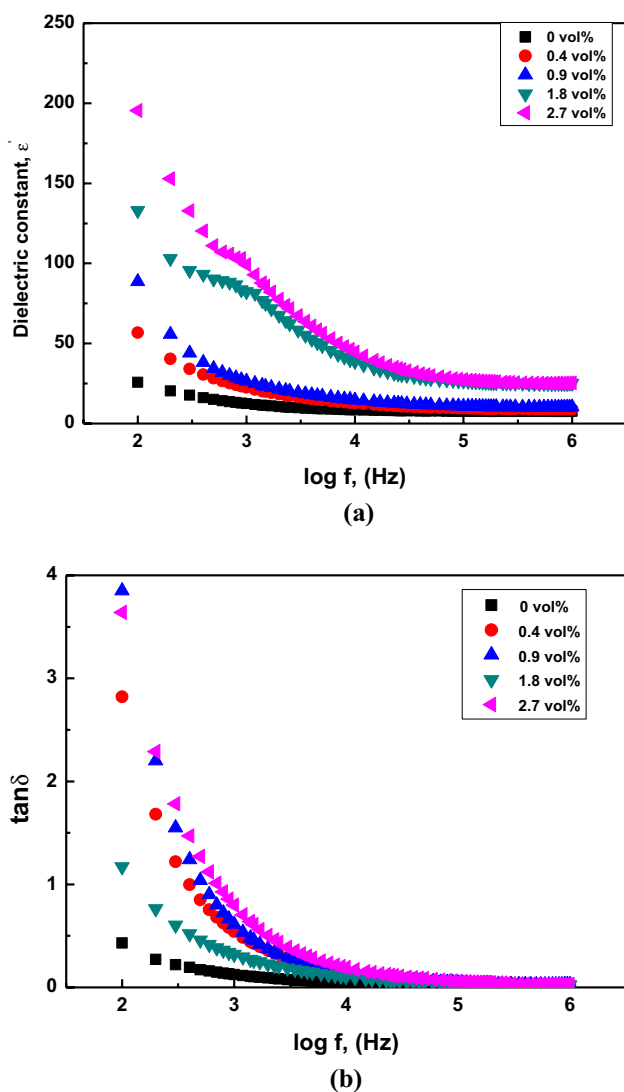


**Fig. 3** Plots of **a**  $\epsilon'$  against frequency at 363 K, **b**  $\tan\delta$  against frequency at 363 K for all nano-composites

dielectric constant ( $\epsilon'$ ) with frequency in our composites can be calculated by using the power law that can be expressed as [48]:

$$\epsilon_{eff} \propto \epsilon_{PVDF}(f_c - f)^{-s} \text{ for } f < f_c \quad (3)$$

In Eq. (3),  $s$  is the critical exponent, while the dielectric constants of composites and PVDF are denoted by  $\epsilon_{eff}$  and  $\epsilon_{PVDF}$  respectively. Also, the volume fraction of filler and corresponding percolation threshold value are represented by  $f$  and  $f_c$ .

We have fitted the experimental data numerically and It has been observed that  $f_c(\text{rGO}) = 1.8 \text{ vol\%}$ . Further, the percolation threshold of rGO/PVDF nano-composites, is an intermediate value for other values obtained for PVDF doped with carbon nano-tubes ( $\sim 8 \text{ vol\%}$ ) [43] or graphene/

PVDF nano-composites ( $\sim 1 \text{ vol\%}$ ), [42, 43, 46]. It is evident from the analysis, the strong dependence of the percolation threshold on the distribution of fillers in a matrix that can be affected by the particles shape, size, orientation, etc. On the other hand the increase in the dielectric constant can be attributed to the fact that near the percolation threshold, according to the existence of PVDF, conductive rGO are still remaining isolative. Consequently, there is a favorable condition for the free charges in graphene to stack at the interface that causes the strong MWS polarization.

The  $\tan \delta$  is an inverse quantity of its quality factor. Therefore, to understand the detailed behavior of a dielectric material, the characterizations of its  $\tan\delta$  spectra are required. Figure 3b shows the variation of the  $\tan \delta$  with a rise in frequency at diverse temperatures. From this Figure, we can see that  $\tan \delta$  decreases with increasing frequency. This could be because of polarization (MWS effect). Another possible reason is the beginning of follow-up by the dipoles to the field variation at higher frequencies [47], while  $\tan \delta$  increases as the concentration of rGo increases in PVDF composites. The percolation effect results d.c. conduction. Consequently, we have observed high values of the dielectric loss tangent or the dissipation factor for all nano-composites at low frequencies. As frequency increases, the reduction in the electronic oscillations takes place that causes a collapse of the induced charges and therefore, the value of  $\tan \delta$  is also decreased. However, for all composites, we observed:  $\tan\delta < 4$  at 1 kHz–1000 kHz, this confirmed its suitability as a high-quality dielectric material, which is suitable for several applications [48, 49]. Generally, the higher dielectric constants and the smaller dielectric loss factor are the typical behavior for the rGO/PVDF nano-composites.

### 3.3 Electric modulus

In composite polymeric materials, interfacial polarization is related to the change of the dielectric constant with low frequencies and high temperatures. According to the above observation, the modulus formalism can be used to analyze the electrical conductivity in an ionic polymeric material, and also to suppress the signal intensity associated with the electrode polarization, emphasizing the small features at high frequencies [50]. For the determination of the complex electric modulus ( $M^*$ ), which is defined as the inverse of the complex function ( $\epsilon^*$ ) we expressed the dielectric data as:

$$M^* = \frac{1}{\epsilon^*} = \frac{\epsilon'}{\epsilon'^2 + \epsilon''^2} + i \frac{\epsilon''}{\epsilon'^2 + \epsilon''^2} \quad (4)$$

$$M^* = M' + iM'' \quad (5)$$

In the Eq. (5)  $M'$  represents the real parts of the electric modulus while  $M''$  is its imaginary part. The frequency dependence of both components for rGO doped PVDF films

at 363 K show that the values of  $M'$  increase with increasing frequency, [see Fig. 4a].

The ionic materials possess S-shaped dispersion of  $M'$  as a remarkable characteristic [51] The  $M'$  values at a low frequency near the zero point indicate the exclusion of the electrode polarization for the present samples. From the observed behavior, it is evident that the role of the electrode polarization becomes dominant at high temperatures and low frequencies. The polarization is influenced by *rGO* within the PVDF matrix and consequently the electrical conductivity and dielectric permittivity. The interfacial polarization or the Maxwell–Wagner–Sillars (MWS) effect is observed in PVDF/*rGO* nano-composites due to the existence of interfaces. This further causes an increase in  $M'$  or  $\epsilon'$ . The gathering of charges at the interfaces is responsible for this phenomenon heterogeneous media [52]. In Fig. 4b for  $M''$  spectra, a peak structure is observed that shifts towards higher frequency region

with increasing doping due to the contribution of interfacial polarization. With the rise in frequency side of the peak, the orientation polarization is reduced because it requires extra time to move as compared to electronic and ionic polarization. This causes a reduction in the polarization. On the other hand at high-frequency side, which corresponds to the interfacial, the charges can only carry out the localized motion since their response to the alternating electric field is negligible [53]. The interfacial polarization mechanism and dipolar relaxation could be responsible for the observed behavior of the dispersion at low and high frequencies respectively [54]. As a general feature, the bell shape of the peak in  $M''$  is atypical for ionic behavior. Additionally, the temperature-dependent hopping of the conduction mechanism can be understood by the spectrum of  $M''$  [55].

The dielectric relaxation time  $\tau_m$  (reported in Table 1) measures the time required for the electric charges of any material to become neutralized during the conduction process. The values of the dielectric relaxation time can be expressed as following equation [56]:

$$\tau_m = \frac{1}{2\pi f_m} \tag{6}$$

here  $f_m$  is the peak-relaxation frequency. It was found that the composition determines strongly the value of relaxation time and it decreases after adding *rGO*. Generally, this decrease in  $\tau_m$  suggests the facilitation of local chain dynamics of PVDF was facilitated after the addition of *rGO* chains [57].

### 3.4 A.C. electrical conductivity

At different temperatures, a.c. conductivity behavior of the present materials can be expressed as:

$$\sigma_{ac} = 2\pi f \epsilon_o \epsilon'' \tag{7}$$

Here  $\epsilon_o$  is the free space permittivity and  $\epsilon''$  is the dielectric loss.

Figure 5 demonstrates the variation of  $\ln \sigma_{ac}$  versus  $\ln \omega$  of the films at a 363 K. The inset of Fig. 5 show that when the highly conductive materials (*rGO*) are filled in nano-composites, their conductivity rises appreciably.

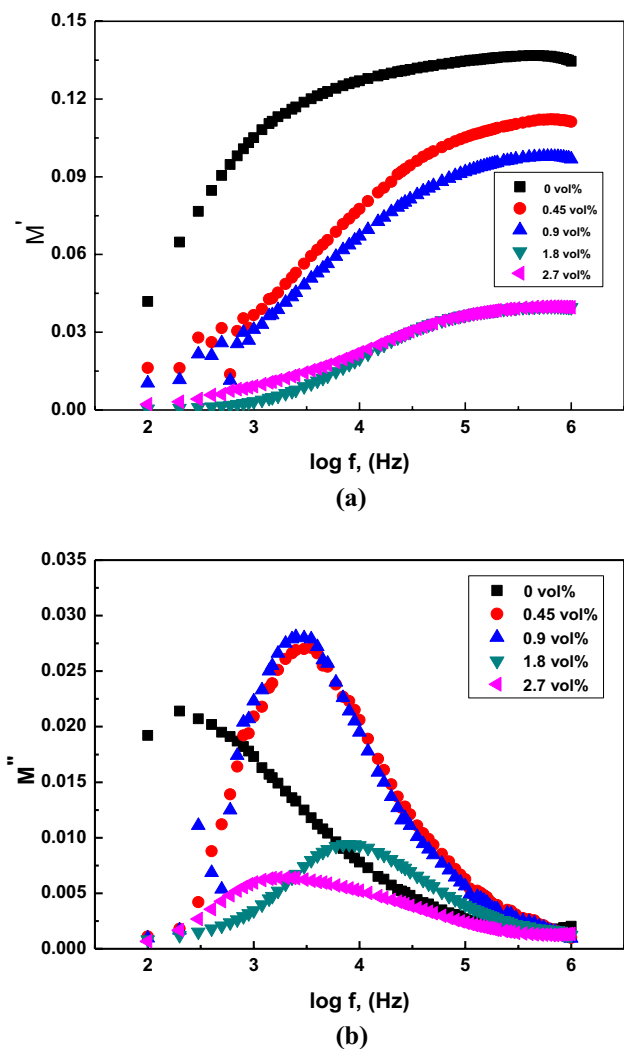
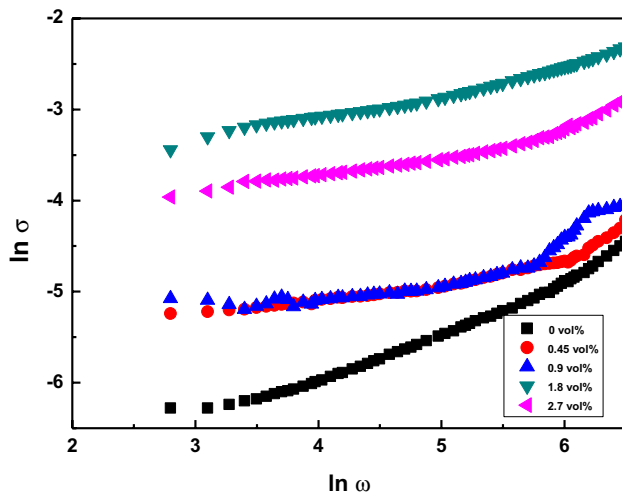


Fig. 4 Frequency-dependent plots of a  $M'$  and b  $M''$  of the PVDF/*rGO*nano-composite films at 363 K

Table 1 Variation of the activation energy  $\Delta E_{ac}$  and the relaxation time  $\tau_m$  with *rGO* content

| PVDF/ <i>rGO</i> (vol%) | $\Delta E_{ac}$ (eV) at 10 KHz | $\Delta E_{ac}$ (eV) at 100 KHz | $\tau_m$ (s)          |
|-------------------------|--------------------------------|---------------------------------|-----------------------|
| 0                       | 0.22                           | 0.16                            | $7.96 \times 10^{-4}$ |
| 0.45                    | 0.21                           | 0.12                            | $1.77 \times 10^{-4}$ |
| 0.9                     | 0.18                           | 0.10                            | $1.33 \times 10^{-4}$ |
| 1.8                     | 0.14                           | 0.08                            | $1.59 \times 10^{-4}$ |
| 2.7                     | 0.13                           | 0.81                            | $2.65 \times 10^{-4}$ |



**Fig. 5** Plots of  $\ln \sigma$  and  $\ln \omega$  for all nano-composites at 363 K

Conductivity appears to be frequency dependent. It was found that beyond a definite point, the conductivity shows exponential variation with frequency [58]. Further, the common behavior of the d.c. conductivity at low-frequency range, in disordered solids and polymeric materials, may be described by the self-styled ‘a.c. universality law’. This type of behavior has also been reported and analyzed as a strong indicator of charge migration through the hopping mechanism [59]. PVDF/rGO systems exhibited relatively higher values of conductivity, which was in general altered with rGO loading, that recovered the ability of conductivity [60]. This behavior infers that the dopant molecules start bridging the gap on increasing the dopant concentration. Further, the applied field increases by means of the electronic jump between localized states as a function of the a.c. activation energy. This causes the separation of the two localized states and the reduction of the potential barrier between them [47].

### 3.5 Effect of the temperature on the dielectric behavior of the PVDF/rGO films

The frequency-dependent  $\epsilon'$  and  $\tan \delta$  spectra of 1.8 vol% PVDF/rGO nano-composite film at various temperatures are shown in Fig. 6.

It is clear that the value of the  $\epsilon'$  is increased with increasing temperature due to thermal agitation, which facilitates the orientational freedom of the polar parts of the PVDF chain [61]. To characterize the thermally activated dielectric polarization behavior of the nano-composite films, the variation of  $\epsilon'$  with the temperature at various frequencies are depicted in Fig. 7.

A relaxation peaks are observed on the nano-composites of the PVDF from the relation between  $\epsilon'$  and the temperature. This behavior has been perceived for attuned blends

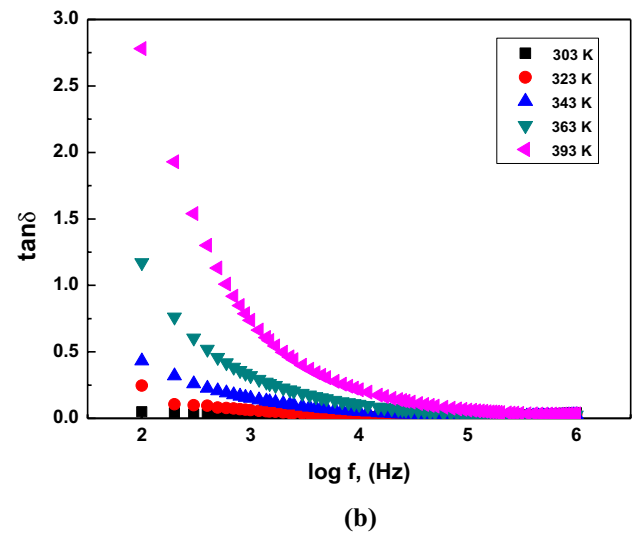
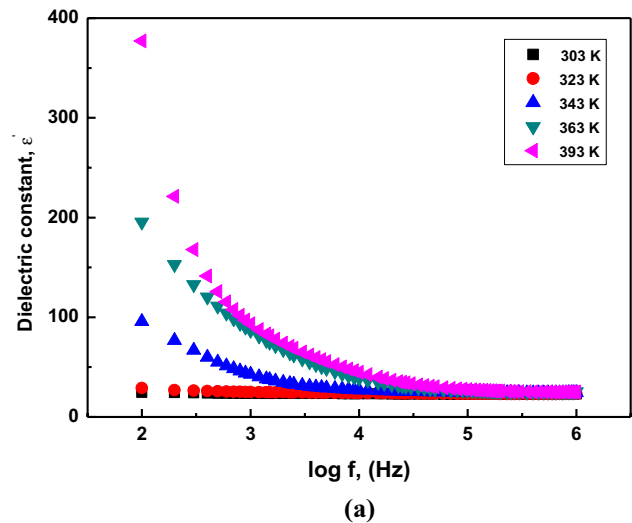


**Fig. 6** Frequency-dependent plots of **a**  $\epsilon'$  and **b**  $\tan \delta$  of the PVDF—1.8 vol% rGO nano-composite films at different temperatures

of PVDF [62, 63] due to the absorption of small thermal energy by the polymeric material at a low temperature and a certain frequency. Thus, the rotation of only a tiny number of dipoles causes an increase in the value of  $\epsilon'$  [64]. With an increase in the temperature, the viscosity decrement in of polymeric films takes place so the dipoles can align conveniently along the applied electric field. Also, enough thermal energy is taken by chain segments to execute rotational motion and to enhance the polarization process [65–67]. Figure 6b shows the increment in  $\tan \delta$  values of the nano-composite films with increasing temperature at low frequencies, but above 100 kHz, the  $\tan \delta$  values were almost temperature independent.

The frequency-dependent  $M'$  and  $M''$  spectra of the PVDF—1.8 vol% rGO film at various temperatures are presented in Fig. 8. We found that the  $M'$  values of the

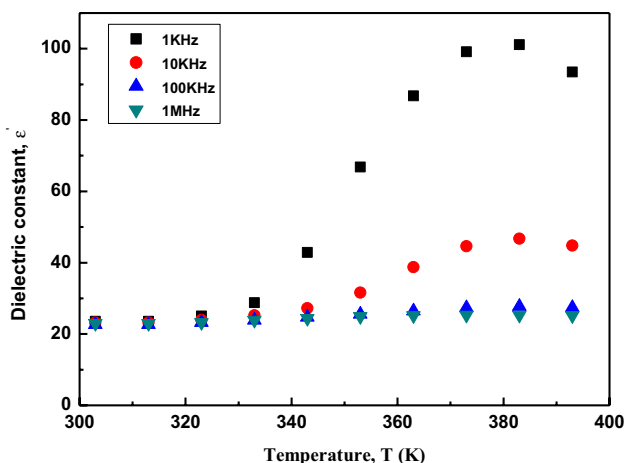


Fig. 7 Temperature dependent  $\epsilon'$  values of the PVDF—1.8 vol% rGO nano-composite films at different frequencies

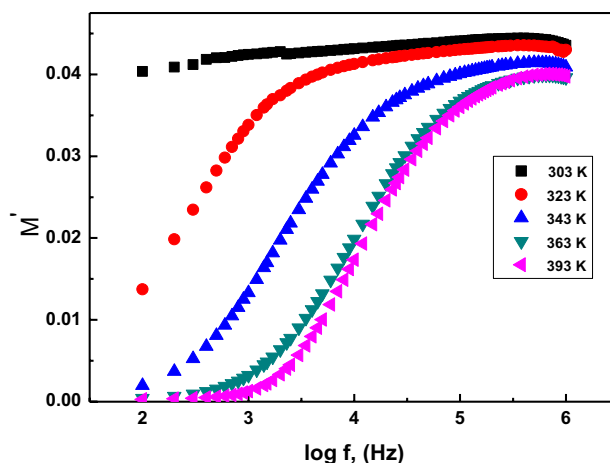
nano-composite films at a constant frequency decreased with increasing temperature, whereas, the  $M''$  spectra exhibited a modulus relaxation peak in the intermediate frequency range. The  $\sigma_{ac}$  spectra of the PVDF—1.8 vol% rGO nano-composite films at different temperatures are depicted in Fig. 9a. As shown in the figure, there was some increase in the  $\sigma_{ac}$  values at lower frequencies with increasing temperature, but at higher frequencies, the increase was insignificant for the nano-composite film.

The behavior of the curves clearly indicates that the a.c. conductivity is responsive to temperature. This type of behavior may be due to the rise in segmental mobility of polymeric chains due to temperature dependence of the specific volume of the polymer. In the localized state, the hopping of the charge carriers and the excitation of charge carriers to these states in the conduction band are the factors that govern the dependence of conductivity on frequency/temperature dependence.

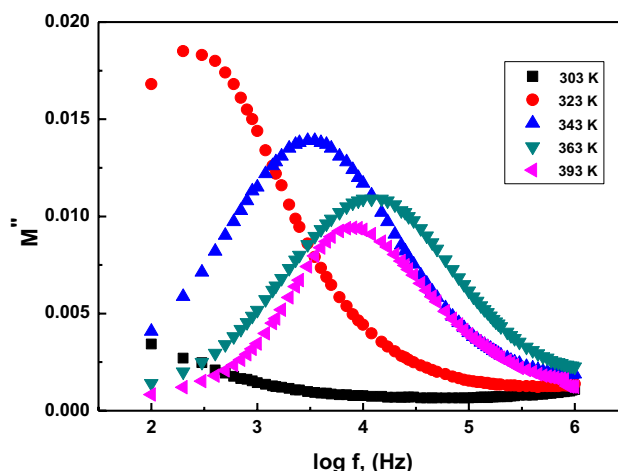
Generally the a.c. conductivity is expressed as:

$$\sigma_{ac}(\omega) = A\omega^S \tag{8}$$

here  $A$  is a pre-exponential factor and  $S$  is the frequency exponent. We determined the value of  $S$  from the slopes of the linear plots of a.c. conductivity against the frequency (see Fig. 10). The increase in a.c. conductivity with increasing frequency is the signature of additional stability in films. The temperature dependence of the frequency exponent is shown in Fig. 9b. It is observed that the value of exponent  $s$  lies in the range 0.18–0.74, which is less than unity. The observed behavior of “ $s$ ” is in agreement with the theory of correlated barrier hopping model (CBH). According to the CBH theory, the conduction occurs through the bi-polaron hopping process where two polarons simultaneously hop over the potential barrier between two charged defect states that, as for increasing temperature the states are produced



(a)



(b)

Fig. 8 Frequency dependent plots of a  $M'$  and b  $M''$  for the PVDF—1.8 vol% rGO nano-composite films at different temperatures

by thermal excitation. The thermally activated nature of a.c. conduction is displayed by the temperature dependence of  $s$  [68].

The plots of  $\sigma_{ac}$  versus  $1/T$  exhibit the same trend as that of pure PVDF as seen from Fig. 10. The values of  $\sigma_{ac}$  for the doped samples are higher than those obtained for pure PVDF due to the large dipole of rGO content. This can be attributed to the structural modification of the polymeric matrix as a result of the doping. The temperature dependence of  $\sigma_{ac}$  is found to follow the Arrhenius relation which is given by:

$$\sigma_{ac} = \sigma_o \exp\left(-\frac{\Delta E_{ac}}{k_B T}\right) \tag{9}$$

here  $\Delta E_{ac}$  is the activation energy for a.c. electrical conduction. The values of  $\Delta E_{ac}$  for pure PVDF and that with different rGO contt at 10 kHz are calculated and listed in Table 1.

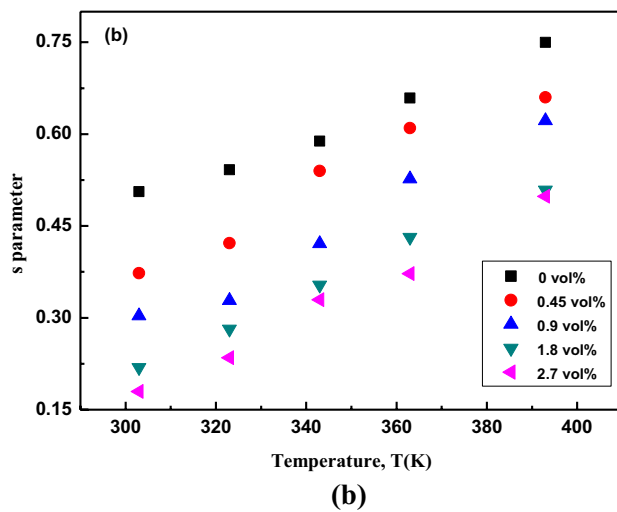
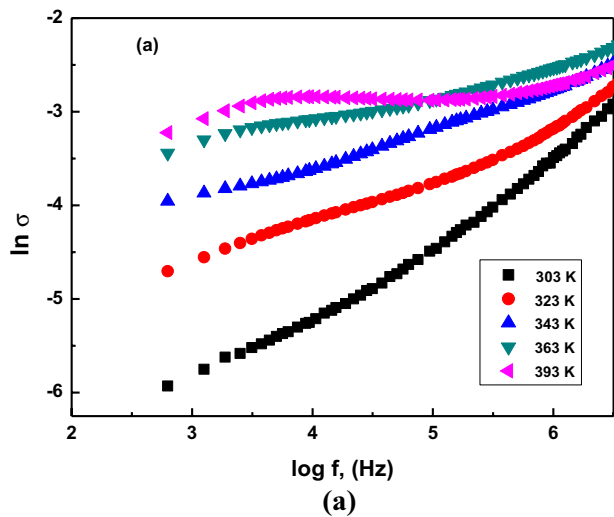


**Fig. 9** **a** Frequency-dependent  $\sigma_{ac}$  of the PVDF—1.8 vol% rGO nano-composite films at different temperatures. **b** The dependence of  $S$  on temperature

The relatively low values of  $\Delta E_{ac}$  recommend the hopping conduction mechanism for a.c. conduction for all samples.

### 3.6 Optimization of dielectric properties: comparison with fillers used in recent studies

In the last one 6 years; various research groups have used diversified materials as fillers with PVDF to improve the dielectric constant and loss [32–41]. Thus, we have compared the dielectric properties of present samples with that of other composites of PVDF with different fillers (see Table 2) for the better understanding of the role of the rGo in the present study. From this table, one can observe that the PVDF/

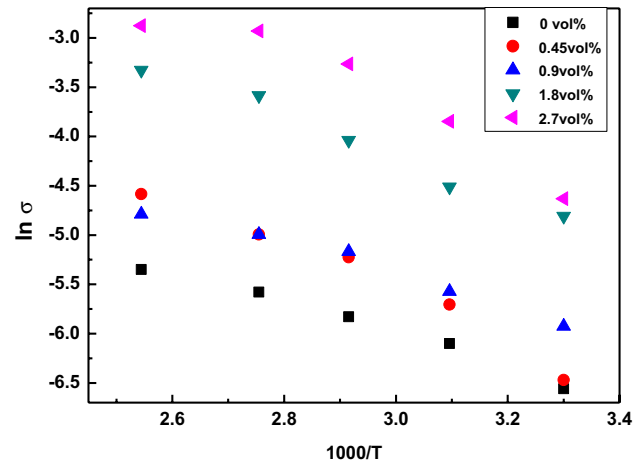


**Fig. 10** The relation between  $\ln \sigma_{ac}$  and  $1/T$  for PVDF nano-composites at  $f = 10$  KHz

rGO composites provide better optimization of the dielectric properties as compared to most of the fillers shown in table.

### 3.7 Compensation effect (Meyer–Neldel rule) in thermally activated a.c. conduction

Knowing the values of activation energy  $\Delta E_{ac}$  and pre-factor  $\ln \sigma_o$  from the slopes of Arrhenius plots of pure PVDF, we have plotted the graphs of  $\ln \sigma_o$  against  $\Delta E_{ac}$ . Such plots are shown in Fig. 11 for 0.9 vol% and 1.8 vol% rGO/PVDF. From this figure, it is clear that  $\ln \sigma_o$  varies linearly with  $\Delta E_{ac}$ ; thereby indicating that  $\ln \sigma_o$  and  $\Delta E_{ac}$  are related to each other according to Meyer–Neldel rule [69]:

$$\sigma_o = \sigma_{oo} \exp \left( + \frac{\Delta E_{ac}}{k_B T_o} \right) \quad (10)$$

Similar plots were observed for the other two samples. The linear relation  $\ln \sigma_o$  and  $\Delta E_{ac}$  between confirms the signature of compensation effect for thermally activated a.c. conduction in present samples of rGO/PVDF. Literature survey shows that such a condition exists if the relaxation time itself follows the compensation effect [70].

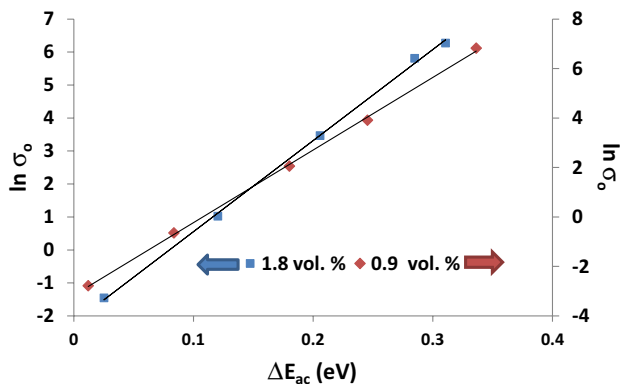
## 4 Conclusions

From FT-IR, SEM spectroscopy and a.c. electrical conductivity measurements, the following conclusions have been drawn. There is an interaction between PVDF and rGO as illustrated from shifts in some bands with a change in their



**Table 2** Comparative analyses of dielectric properties for present study and recently published studies

| Composites Materials of PVDF with different fillers                                 | Filler content | Dielectric constant | Loss tangent | Frequency (Hz) | References   |
|---|----------------|---------------------|--------------|----------------|--------------|
| CaCu <sub>3</sub> Ti <sub>4</sub> O <sub>12</sub>                                   | 55 (vol%)      | ~ 188               | ~0.87        | 1000           | [32]         |
| Spherical Al (20 μm)  | 80 (wt%)       | ~ 135               | ~0.06        | 100            | [33]         |
| Zinc flakes   | 24 (vol%)      | 127                 | 0.19         | 100            | [34]         |
| TiO <sub>2</sub> @CNT   | 1 (wt%)        | 60                  | 0.260        | 100            | [35]         |
| BT@SnO <sub>2</sub>   | 45 (vol%)      | 160                 | 1.350        | 100            | [36]         |
| BT-RGO  | 30 (vol%)      | 67.5                | 0.060        | 1000           | [37]         |
| BT@Fe <sub>3</sub> O <sub>4</sub>   | 40 (vol%)      | 138                 | 0.240        | 100            | [38]         |
| BaTiO <sub>3</sub>  | 30 (vol%)      | ~ 58                | ~0.038       | 1000           | [39]         |
| Nano-barium titanate (NBT)  | 20 (wt%)       | ~ 16.5              | 0.0025       | 1000           | [40]         |
| NBT/Ni(OH) <sub>2</sub>   | 20 (wt%)       | 25                  | ~0.05        | 1000           | [40]         |
| Plate-like (Ba <sub>0.6</sub> Sr <sub>0.4</sub> )TiO <sub>3</sub> (P-BST) particles | 40 (vol%)      | 62.2                | 0.042        | 1000           | [41]         |
| rGO   | 2.7 (vol%)     | 195                 | ~0.7         | 100            | Present work |
| rGO   | 2.7 (vol%)     | 101                 | ~0.7         | 1000           | Present work |

**Fig. 11**  $\ln \sigma_0$  versus  $\Delta E_{ac}$  plots for PVDF—0.9 vol% rGO and PVDF—1.8 vol% rGO nano-composite films

intensities, also clear phase (alpha to beta) transition of PVDF in the existence of rGO was observed by FTIR analysis. SEM images show that rGO were dispersed well in polymeric matrices. The percolation threshold for PVDF/rGO nano-composites was 1.8 vol%. The dielectric properties of PVDF are reinforced with adding rGO. The measurements of Dielectric properties (dielectric constant and loss tangent) reveal that introducing rGO into PVDF matrix facilitates the optimization (high dielectric constant and low loss tangent) of dielectric properties as compared to various other fillers used by diversified groups in recent past.

The dielectric behavior of the nano-composites exhibit relaxation peaks in the values of  $M''$  referred to MWS effects. A.C. conductivity has been found to obey the power law and increases with inverting frequency in the measured temperature. The activation energy and pre-exponential factor for a.c. conduction satisfies the compensation effect (also known as Meyer–Neldel rule). These results are reasonably

well interpreted in the context of the correlated barrier hopping (CBH) model. The present studies indicate that the PVDF/rGO nano-composites synthesized by us are potential materials for high-charge storage capacitive applications in microelectronic devices.

**Acknowledgements** NM wishes to acknowledge the financial assistance received under UPE Programme (Scheme No. 4204).

## References

1. K.S. Novoselo, Electric field effect in atomically thin carbon films. *Science* **306**, 666–669 (2004)
2. D. Chen, H. Feng, J. Li, G. Oxide, Preparation, functionalization, and electrochemical applications. *Chem. Rev.* **112**, 6027–6053 (2012)
3. X. Huang, Z. Yin, S. Wu, X. Qi, Q. He, Q. Zhang, Q. Yan, F. Boey, H. Zhang, Graphene-based materials: synthesis, characterization, properties, and applications. *Small* **7**, 1876–1902 (2011)
4. D. Fan, C. Zhang, J. He, R. Hua, Y. Zhang, Y. Yang, Redox chemistry between graphene oxide and mercaptan. *J. Mater. Chem.* **22**, 18564–18571 (2012)
5. D.R. Dreyer, S. Park, C.W. Bielawski, R.S. Ruoff, The chemistry of graphene oxide. *Chem. Soc. Rev.* **39**, 228–240 (2010)
6. H. Bai, C. Li, G. Shi, Functional composite materials based on chemically converted grapheme. *Adv. Mater.* **23**, 1089–1115 (2011)
7. R. Larciprete, S. Fabris, T. Sun, P. Lacovig, A. Baraldi, S. Lizzit, Dual path mechanism in the thermal reduction of graphene oxide. *J. Am. Chem. Soc.* **133**, 17315–17321 (2011)
8. Y. Xu, Q. Wu, Y. Sun, H. Bai, G. Shi, Three-dimensional self-assembly of graphene oxide and DNA into multifunctional hydrogels. *ACS Nano* **4**, 7358–7362 (2010)
9. O.O. Ekiz, M. Urel, H. Guner, A.K. Mizrak, A. Dana, Reversible electrical reduction and oxidation of graphene oxide. *ACS Nano* **5**, 2475–2482 (2011)

10. S. Stankovich, D.A. Dikin, G.H.B. Dommett, K.M. Kohlhaas, E.J. Zimney, E.A. Stach, R.D. Piner, S.T. Nguyen, R.S. Ruoff, Graphene-based composite materials. *Nature* **442**, 282–286 (2006)
11. L. Seveyrat, A. Chalkha, D. Guyomar, L. Lebrun, Preparation of graphene nanoflakes/polymer composites and their performances for actuation and energy harvesting applications. *J. Appl. Phys.* **111**, 104904 (2012)
12. Z. Wang, J.K. Nelson, H. Hillborg, S. Zhao, L.S. Schadler, Graphene oxide filled nanocomposite with novel electrical and dielectric properties. *Adv. Mater.* **24**, 3134–3137 (2012)
13. C.-W. Nan, Physics of inhomogeneous inorganic materials. *Prog. Mater. Sci.* **37**, 1–116 (1993)
14. Y. Zhen, J. Arredondo, Z. Guang-Lin, Unusual dielectric loss properties of carbon nanotube—polyvinylidene fluoride composites in low frequency region ( $100 \text{ Hz} < f < 1 \text{ MHz}$ ). *Open J. Organic Polym. Mater.* **3**, 99–103 (2013)
15. D. Wang, Y. Bao, J.W. Zha, J. Zhao, Z.M. Dang, G.H. Hu, Improved dielectric properties of nanocomposites based on poly(vinylidene fluoride) and poly(vinyl alcohol)-functionalized graphene. *ACS Appl. Mater. Interfaces* **4**, 6273–6279 (2012)
16. L. Cui, X. Lu, D. Chao, H. Liu, Y. Li, C. Wang, Graphene-based composite materials with high dielectric permittivity via an in situ reduction method. *Phys. Status Solidi (A)* **208**, 459–461 (2011)
17. X.J. Zhang, G.S. Wang, *Proceedings of the 16th International Conference on Nanotechnology*, Sendai, Japan, 2016, pp. 22–25
18. P. Fan, L. Wang, J. Yang, F. Chen, M. Zhong, Graphene/poly(vinylidene fluoride) composites with high dielectric constant and low percolation threshold. *Nanotechnology* **23**, 365702 (2012)
19. T. Kuilla, S. Bhadra, D. Yao, N.H. Kim, S. Bose, J.H.P. Lee, Recent advances in graphene based polymer composites. *Polym. Sci.* **35**, 1350–1375 (2010)
20. H. Kim, A.A. Abdala, C.W. Macosko, Graphene/polymer nanocomposites. *Macromolecules* **43**, 6515–6530 (2010)
21. Z. Xu, C. Gao, In situ polymerization approach to graphene-reinforced nylon-6 composites. *Macromolecules* **43**, 6716–6723 (2010)
22. L. Kan, Z. Xu, C. Gao, General avenue to individually dispersed graphene oxide-based two-dimensional molecular brushes by free radical polymerization. *Macromolecules* **44**, 444–452 (2011)
23. D. Wang, Y. Bao, J.-W. Zhao, Z.-M. Dang, G.-H. Hu, Improved dielectric properties of nanocomposites based on poly(vinylidene fluoride) and poly(vinyl alcohol)-functionalized graphene. *ACS Appl. Mater. Interfaces* **4**, 6273–6279 (2012)
24. W.K. Chee, H.N. Lim, N.M. Huang, I. Harrison, Nanocomposites of graphene/polymers: a review. *RSC Adv.* **5**, 68014–68051 (2015)
25. A. Qin, X. Li, X. Zhao, D. Liu, C. He, Engineering a highly hydrophilic PVDF membrane via binding  $\text{TiO}_2$  nanoparticles and a PVA layer onto a membrane surface. *ACS Appl. Mater. Interfaces* **7**, 8427–8436 (2015)
26. T. Wu, B. Zhou, T. Zhu, J. Shi, Z. Xu, C. Hu, J. Wang, Facile and low-cost approach towards a PVDF ultrafiltration membrane with enhanced hydrophilicity and antifouling performance via graphene oxide/water-bath coagulation. *RSC Adv.* **5**, 7880–7889 (2015)
27. C. Zhao, X. Xu, J. Chen, G. Wang, F. Yang, Highly effective antifouling performance of PVDF/graphene oxide composite membrane in membrane bioreactor (MBR) system. *Desalination* **340**, 59–66 (2014)
28. J. Yu, Y. Wang, W. Xiao, Enhanced photoelectrocatalytic performance of  $\text{SnO}_2/\text{TiO}_2$  rutile composite films Yang. *J. Mater. Chem. A* **1**, 10727–10735 (2013)
29. Z.-W. Ouyang, E.-C. Chen, T.-M. Wu, Thermal stability and magnetic properties of polyvinylidene fluoride/magnetite nanocomposites. *Materials* **8**, 4553–4564 (2015)
30. A.A. Issa, M.A. Al-Maadeed, A.S. Luyt, M. Mrlik, M.K. Hassan, Investigation of the physico-mechanical properties of electrospun PVDF/cellulose (nano) fibers. *J. Appl. Polym. Sci.* **133**, 43594 (2016)
31. A. Al-Saygh, D. Ponnamma, M. Al., P. Maadeed, P. Vijayan, A. Karim, M.K. Hassan, Flexible pressure sensor based on PVDF nanocomposites containing reduced graphene oxide-titania hybrid nanolayers. *Polymers* **9**, 33 (2017)
32. P. Thomas, K.T. Varughese, K. Dwarakanath, K.B.R. Varma, Dielectric properties of Poly(vinylidene fluoride)/ $\text{CaCu}_3\text{Ti}_4\text{O}_{12}$  composites. *Compos. Sci. Technol.* **70**, 539–545 (2010)
33. W. Zhou, J. Zuo, W. Ren, Thermal conductivity and dielectric properties of Al/PVDF composites. *Compos. A* **43**, 658–664 (2012)
34. Y. Deng, Y. Zhang, Y. Wang, M. Li, J. Yuan, J. Bai, A facile way to fabricate novel 2–3-type composites based on zinc powders and polyvinylidene fluoride with enhanced dielectric properties. *Composites Part A* **43**, 842–846 (2012)
35. L. Yang, J.H. Qiu, H.L. Ji, K.J. Zhu, J. Wang, Enhanced dielectric and ferroelectric properties induced by  $\text{TiO}_2$ @MWCNTs nanoparticles in flexible poly(vinylidene fluoride) composites. *Composites Part A* **65**, 125–134 (2014)
36. J.W. Zha, X. Meng, D. Wang, Z.M. Dang, R.K.Y. Li, Dielectric properties of poly(vinylidene fluoride) nanocomposites filled with surface coated  $\text{BaTiO}_3$  by  $\text{SnO}_2$  nanodots. *Appl. Phys. Lett.* **104**, 072906 (2014)
37. Y. Li, Y. Shi, F. Cai, J. Xue, F. Chen, Q. Fu, Graphene sheets segregated by barium titanate for polyvinylidene fluoride composites with high dielectric constant and ultralow loss tangent. *Composites Part A* **78**, 318–326 (2015)
38. C. Zhang, Q. Chi, J. Dong, Y. Cui, X. Wang, L. Liu, Q. Lei, Enhanced dielectric properties of poly(vinylidene fluoride) composites filled with nano iron oxide-deposited barium titanate hybrid particles. *Sci. Rep.* **6**, 33508 (2016)
39. R. Li, Z. Zhao, Z. Chen, J. Pei, Novel  $\text{BaTiO}_3$ /PVDF composites with enhanced electrical properties modified by calcined  $\text{BaTiO}_3$  ceramic powders. *Mater. Express* **7**, 536–540 (2017)
40. Y. Yang, Z. Li, W. Ji, C. Sun, H. Deng, Q. Fu, Enhanced dielectric properties through using mixed fillers consisting of nano-barium titanate/nickel hydroxide for polyvinylidene fluoride based composites. *Composites Part A* **104**, 24–31 (2018)
41. F. Li Wang, J. Gao, K. Xu, J. Zhang, M. Kong, H. Reece, Yan, Enhanced dielectric tunability and energy storage properties of platelike ( $\text{Ba}_{0.6}\text{Sr}_{0.4}$ ) $\text{TiO}_3$ /poly(vinylidene fluoride) composites through texture arrangement. *Compos. Sci. Technol.* **158**, 112–120 (2018)
42. Z.M. Dang, L. Wang, Y. Yin, Q. Zhang, Q.Q. Lei, Giant dielectric permittivities in functionalized carbon-nanotube/electroactive-polymer nanocomposites. *Adv. Mater.* **19**, 852–857 (2007)
43. F. He, S. Lau, H.L. Chan, J.T. Fan, High dielectric permittivity and low percolation threshold in nanocomposites based on poly(vinylidene fluoride) and exfoliated graphite nanoplates. *Adv. Mater.* **21**, 710–715 (2009)
44. Z.-M. Dang, J.-K. Yuan, J.-W. Zha, T. Zhou, S.-T. Li, G.-H. Hu, Fundamentals, processes and applications of high permittivity polymer-matrix composites. *Prog. Mater. Sci.* **57**, 660–723 (2012)
45. H.X. Tang, G.J. Ehlert, Y.R. Lin, H.A. Sodano, Highly efficient synthesis of graphene nanocomposites. *Nano Lett.* **12**, 84–90 (2012)
46. X.L. Xu, C.J. Yang, J.H. Yang, T. Huang, Y. Wang, Z.-W. Zhou, Excellent dielectric properties of poly(vinylidene fluoride) composites based on partially reduced graphene oxide. *Composites Part B* **109**, 91–100 (2017)
47. I.S. Elashmawi, L.H. Gaabour, Raman, morphology and electrical behavior of nanocomposites based on PEO/PVDF with multi-walled carbon nanotubes. *Results Phys.* **5**, 105–110 (2015)

48. Z.-M. Dang, T. Zhou, S.-H. Yao, J.-K. Yuan, J.-W. Zha, H.-T. Song, J.-Y. Li, Q. Chen, W.T. Yang, J. Bai, Advanced calcium copper titanate/polyimide functional hybrid films with high dielectric permittivity. *Adv. Mater.* **21**, 2077–2082 (2009)
49. J.-K. Yuan, W.-L. Li, S.-H. Yao, Y.-Q. Lin, A. Sylvestre, J. Bai, High dielectric permittivity and low percolation threshold in polymer composites based on SiC-carbon nanotubes micro/nano hybrid. *Appl. Phys. Lett.* **98**, 032901 (2011)
50. H. Lu, X. Zhang, H. Zhang, Influence of the relaxation of Maxwell-Wagner-Sillars polarization and dc conductivity on the dielectric behaviors of nylon 1010. *J. Appl. Phys.* **100**, 054104 (2006)
51. A. Hassen, T. Hanafy, S. El-Sayed, A. Himanshu, Dielectric relaxation and alternating current conductivity of polyvinylidene fluoride doped with lanthanum chloride. *J. Appl. Phys.* **110**, 114119 (2011)
52. S. El-Sayed, T.A. Abdel-Baset, A. Hassen, Dielectric properties of PVDF thin films doped with 3 wt.% of  $RCl_3$  ( $R = Gd$  or  $Er$ ). *AIP Adv.* **4**, 037114 (2014)
53. G.A. Samara, F. Baur, The effects of pressure on the  $\beta$  molecular relaxation and phase transitions of the ferroelectric copolymer  $P(VDF_{0.7}TrFe_{0.3})$ . *Ferroelectrics* **135**, 385–399 (1992)
54. J. Ross Macdonald, Simplified impedance/frequency-response results for intrinsically conducting solids and liquids. *J. Chem. Phys.* **61**, 3977–3996 (1974)
55. A.C. Lopes, C.M. Costa, R.S. Serra, I.C. Neves, J.L.G. Ribelles, S.L. Mendez, Dielectric relaxation, ac conductivity and electric modulus in poly(vinylidene fluoride)/NaY zeolite composites. *Sol. Stat. Ionics* **235**, 42–50 (2013)
56. P. Thomas, S. Satapathy, K. Dwarakanath, K.B. Varma, Dielectric properties of poly(vinylidene fluoride)/ $CaCu_3Ti_4O_{12}$  nanocrystal composite thick films. *Express Polym. Lett.* **4**, 632–643 (2010)
57. J. Tahalyani, K.K. Rahangdale, K. Balasubramanian, The dielectric properties and charge transport mechanism of  $\pi$ -conjugated segments decorated with intrinsic conducting polymer. *RSC Adv.* **6**, 69733–69742 (2016)
58. G.C. Psarras, Hopping conductivity in polymer matrix-metal particles composites. *Composites Part A* **37**, 1545–1553 (2006)
59. G.N. Tomara, P.K. Karahaliou, G.C. Psarras, S.N. Georga, C.A. Krontiras, Dielectric relaxation mechanisms in polyoxymethylene/polyurethane/layered silicates hybrid nanocomposites. *Eur. Polym. J.* **95**, 304–313 (2017)
60. W. Tong, Y. Zhang, L. Yu, X. Luan, Q. An, Q. Zhang, F. Lv, P.K. Chu, B. Shen, Z. Zhang, Novel method for the fabrication of flexible film with oriented arrays of graphene in poly(vinylidene fluoride-co-hexafluoropropylene) with low dielectric loss. *J. Phys. Chem. C* **118**, 10567–10573 (2014)
61. S. Mahrous, Dielectric analysis of the  $\alpha$ -relaxation of PVC stabilized with cadmium laurate. *Polym. Int.* **40**, 261–267 (1996)
62. G.K. Narula, P.K.C. Pillai, Dielectric and TSC study in a semi-compatible solution-mixed PVDF-PMMA blend. *J. Mater. Sci. Lett.* **8**, 608–611 (1989)
63. V. Rao, P.V. Ashokan, M.H. Shridhar, Studies of dielectric relaxation and a.c conductivity in cellulose acetate hydrogen phthalate-poly(methyl methacrylate) blends. *Mater. Sci. Eng. A* **281**, 213–220 (2000)
64. A.M. El Sayed, Synthesis and controlling the optical and dielectric properties of CMC/PVA blend via  $\gamma$ -rays irradiation. *Nucl. Instrum. Methods Phys. Res. B* **321**, 41–48 (2014)
65. A. Belal, M. Amin, H. Hassan, A. Abd El-Mongy, B. Kamal, K. Ibrahim, The role of  $BaTiO_3$  on the dielectric properties of polyvinyl chloride. *Phys. Stat. Solidi (A)* **144**, 53–57 (1994)
66. A. Hassen, A.M. El Sayed, W.M. Morsi, S. El-Sayed, Influence of  $Cr_2O_3$  nanoparticles on the physical properties of polyvinyl alcohol. *J. Appl. Phys.* **112**, 093525 (2012)
67. T.A. Hanafy, Dielectric relaxation and alternating-current conductivity of gadolinium-doped poly(vinyl alcohol). *J. Appl. Polym. Sci.* **108**, 2540–2549 (2008)
68. H.M. Ragab, Spectroscopic investigations and electrical properties of PVA/PVP blend filled with different concentrations of nickel chloride. *Physica B* **406**, 3759–3767 (2011)
69. N. Mehta, Meyer-Neldel rule in chalcogenide glasses: recent observations and their consequences. *Curr Opin Solid State Mater. Sci.* **14**, 95–106 (2010)
70. A.-W. Fouad, Signature of the Meyer-Neldel rule on the correlated barrier-hopping model. *J. Appl. Phys.* **91**, 265–270 (2002)